HHS Public Access
Author manuscript
Dev Biol. Author manuscript; available in PMC 2018 September 01.

Published in final edited form as:
Dev Biol. 2017 September 01; 429(1): 225–239. doi:10.1016/j.ydbio.2017.06.024.

Pnrc2 regulates 3′UTR-mediated decay of segmentation clock-associated transcripts during zebrafish segmentation

Thomas L. Gallagher[1,2,1], **Kiel T. Tietz**[1,2,1], **Zachary T. Morrow**[1], **Jasmine M. McCammon**[3,*], **Michael L. Goldrich**[3], **Nicolas L. Derr**[1], and **Sharon L. Amacher**[1,2,4,5,‡]

[1]Molecular Genetics, The Ohio State University, Columbus, OH, 43210

[2]Center for RNA Biology, The Ohio State University, Columbus, OH, 43210

[3]Molecular and Cell Biology, University of California, Berkeley, CA, 94720

[4]Biological Chemistry and Pharmacology, The Ohio State University, 43210

[5]Center for Muscle Health and Neuromuscular Disorders, The Ohio State University, 43210

Abstract

Vertebrate segmentation is controlled by the segmentation clock, a molecular oscillator that regulates gene expression and cycles rapidly. The expression of many genes oscillates during segmentation, including *hairy/Enhancer of split-related* (*her* or *Hes*) genes, which encode transcriptional repressors that auto-inhibit their own expression, and *deltaC* (*dlc*), which encodes a Notch ligand. We previously identified the *tortuga (tor)* locus in a zebrafish forward genetic screen for genes involved in cyclic transcript regulation and showed that cyclic transcripts accumulate post-splicing in *tor* mutants. Here we show that cyclic mRNA accumulation in *tor* mutants is due to loss of *pnrc2*, which encodes a proline-rich nuclear receptor co-activator implicated in mRNA decay. Using an inducible *in vivo* reporter system to analyze transcript stability, we find that the *her1* 3′UTR confers Pnrc2-dependent instability to a heterologous transcript. *her1* mRNA decay is Dicer-independent and likely employs a Pnrc2-Upf1-containing mRNA decay complex. Surprisingly, despite accumulation of cyclic transcripts in *pnrc2*-deficient embryos, we find that cyclic protein is expressed normally. Overall, we show that Pnrc2 promotes 3′UTR-mediated decay of developmentally-regulated segmentation clock transcripts and we uncover an additional post-transcriptional regulatory layer that ensures oscillatory protein expression in the absence of cyclic mRNA decay.

[‡]Author for correspondence (amacher.6@osu.edu).
[*]Present address: Whitehead Institute for Biomedical Research, Cambridge, MA 02142
[1]Authors contributed equally to this work.

COMPETING INTERESTS

The authors declare no competing or financial interests.

AUTHOR CONTRIBUTIONS

T.L.G., K.T.T., Z.T.M, J.M.M., M.L.G., N.L.D., and S.L.A. performed experiments and analyzed data. All authors contributed intellectually and discussed the data and manuscript. T.L.G. wrote the manuscript and all authors participated in the editing process.

Keywords

Hes/her; RNA decay; oscillations; Tortuga; somitogenesis; cyclic expression

INTRODUCTION

Ultradian oscillatory circuits, with periods of minutes or hours, are pervasive in biological systems (Levine et al, 2013; Purvis and Lahav, 2013; Sonnen and Aulehla, 2014). Oscillatory expression encodes an enormous amount of potential information; for example, there can be critical information in the number, amplitude, duration, or frequency of oscillations, as well as signal integration among multiple oscillators that collectively determine cellular response. A well-studied example of biological oscillation is the segmentation clock, a rapid molecular oscillator that generates periodic expression in developing embryos (Hubaud and Pourquié, 2014; Oates et al, 2012; Pourquié 2011). The segmentation clock controls vertebrate somitogenesis, the process by which the mesoderm is sequentially divided into segmental units called somites that later give rise to vertebrae and ribs, body musculature, and dermis. Molecular oscillations during vertebrate segmentation were first described for *c-hairy1*, a chick homolog of the *Drosophila* pair rule gene *hairy*. In chick embryos, *c-hairy1* expression cycles in the presomitic mesoderm (PSM) and the period of each cycle corresponds with segment formation (Palmeirim et al, 1997). Since its discovery, *c-hairy1* orthologs have been identified in many vertebrate species. Mouse orthologs *Hes1* and *Hes7* and zebrafish orthologs *her1* and *her7* cycle dynamically in the PSM (2 hours in mouse and 30 minutes in zebrafish) and are required for proper segmentation (Bessho et al, 2001; Bessho et al, 2003; Gajewski et al, 2003; Harima et al, 2014; Henry et al, 2002; Hirata et al, 2002; Holley et al, 2000; Oates et al, 2002; Takke and Campos-Ortega, 1999). In zebrafish, overexpression of *her* mRNA is associated with severe segmentation defects (Giudicelli et al, 2007; Takke and Campos-Ortega, 1999), and more recent work has confirmed that oscillatory expression is important for somite formation (Soza-Ried et al, 2014).

Several studies have explored activation and negative feedback inhibition of oscillatory transcription (e.g., Bessho et al, 2003; Giudicelli et al, 2007; González et al, 2013; Hirata et al, 2002; Lewis, 2003; Schwendinger-Schreck et al, 2014). More recently, studies have also investigated post-transcriptional mechanisms regulating transcript processing and clearance (Cibois et al, 2010; Fujimuro et al, 2014; Hanisch et al, 2013; Nitanda et al, 2014). Notable are studies that indicate splicing is a critical parameter (Harima et al, 2013; Takashima et al, 2011), mRNA export is a rate-limiting step (Hoyle and Ish-Horowicz, 2013), translational delays contribute to traveling waves of expression (Ay et al, 2014), oscillatory protein turnover is required for transcriptional and post-transcriptional clock function (Williams et al, 2016), cyclic transcript 3′UTRs can promote decay (Delaune et al, 2012, Fujimuro et al, 2014; Giudicelli et al, 2007), and miRNAs regulate decay of some cyclic transcripts (Bonev et al, 2012; Riley et al, 2013; Tan et al, 2012; Wong et al, 2015). Rapid clearance of cyclic transcripts likely occurs using mRNA decay machinery that promotes deadenylation, 5′ cap removal, and/or exonucleolytic cleavage of natural, non-aberrant transcripts (Garneau et al, 2007; Ghosh and Jacobson, 2010; Houseley and Tollervey, 2009; Lykke-Andersen and

Jensen, 2015; Schoenberg and Maquat, 2012), though how cyclic transcripts are efficiently targeted and cleared remains largely unknown.

In a forward genetic screen, we discovered a zebrafish mutant, *tortuga* (*tor*), with post-transcriptional accumulation of clock-associated transcripts, such as *her1*, *her7*, *deltaC* (*dlc*), and *deltaD* (*dld*) (Dill et al, 2005). For simplicity, we refer collectively to clock-associated transcripts as cyclic through the body of this work, although *deltaD* (*dld*) expression does not oscillate (Holley et al, 2000). Normally, cyclic expression appears as dynamic stripes of expression in the anterior PSM due to rapid oscillatory transcription followed by rapid mRNA decay; in *tortuga* mutants, the accumulation of cyclic transcripts obscures the striped expression pattern even though cyclic transcription appears normal (Dill et al., 2005). Although many genes are deleted in the *tortuga* deficiency allele, we hypothesized that loss of *pnrc2* specifically leads to accumulation of segmentation clock transcripts in *tortuga* mutants. PNRC2 was first identified in a yeast two-hybrid screen of a human mammary gland cDNA library using mouse steroidogenic factor 1 (SF1) as bait (Zhou and Chen, 2001) and subsequently shown to interact with several classes of steroid hormone receptors *in vitro* (Hentschke and Borgmeyer, 2003; Zhou and Chen, 2001; Zhou et al, 2006). More recently, Pnrc2 has been described as an adapter protein of mRNA decay machinery that promotes decay of reporter mRNA containing a premature termination codon (PTC) (Cho et al, 2009; Cho et al, 2012; Cho et al, 2013a; Cho et al, 2013b; Cho et al, 2015; Lai et al, 2012; Mugridge et al, 2016). We show here that Pnrc2 is required for rapid turnover of cyclic transcripts during vertebrate segmentation. We demonstrate that the *her1* 3′UTR confers Pnrc2-dependent instability, extending previous work in cultured cells that shows that Pnrc2 affects mRNA stability of synthetic PTC-containing reporters via NMD (Cho et al, 2009; Lai et al, 2012). We find that Pnrc2-mediated decay of *her1* transcripts does not require Dicer-dependent miRNAs and likely occurs via interaction with the mRNA decay factor Upf1. Our work identifies novel targets regulated by Pnrc2 in a developmental context and implicates the existence of an additional post-transcriptional regulatory mechanism that ensures proper oscillatory protein expression.

MATERIALS & METHODS

Animal stocks and husbandry

Adult zebrafish strains (*Danio rerio*) were kept at 28.5°C on a 14 hour (h) light/10h dark cycle and obtained by natural spawning or *in vitro* fertilization, and were staged according to Kimmel et al (1995). The *tortuga* (*tor*) mutant allele, *b644*, was isolated in a screen designed to identify mutations that disrupt segmental gene expression (Dill et al, 2005). The segmentation clock reporter line, $Tg(her1{:}her1\text{-}Venus)^{bk15}$, was generated previously to visualize cyclic gene expression (Delaune et al, 2012; Shih et al, 2015). The stable *hsp70l:Venus-her1* 3′UTR reporter line and the $pnrc2^{oz22}$ allele, described below, were generated in this study. Animal experiments were performed in accordance with institutional and national guidelines and regulations and were approved by the UC Berkeley and Ohio State University Animal Care and Use Committees.

Recombination mapping

Initial recombination mapping of the *tor*^{b644} deletion allele was performed using bulk segregant analysis (Postlethwait et al, 1994) to identify polymorphic CA-repeat microsatellite markers showing biased representation in pooled genomic DNA from haploid progeny derived from an F1 AB/SJD hybrid female carrying the *tor*^{b644} allele. Recombination frequency for linked markers was calculated by analyzing marker segregation among many mutant and wildtype F1 hybrid individuals. The extent of the *tor*^{b644} deletion was defined as described in Results. Mapping marker locations and sequences are available at the Zebrafish Model Organism Database (ZFIN), University of Oregon, Eugene, OR 97403-5274; URL: http://zfin.org/.

BAC injection

A total of 4 BACs spanning the *tortuga*^{b644} deletion were injected at doses of 0.4–30 pg directly into 1-cell stage embryos from a cross between heterozygous *tor*^{b644} carriers. At 18 hpf, embryos in each BAC-injected clutch were sorted for neural degeneration (a visible *tor* phenotype), and then fixed in 4% PFA for 5 hours at room temperature, processed for *her1* in situ hybridization, scored for *her1* expression phenotype, and PCR genotyped. Only BAC AL844887 restored normal *her1* expression in *tor*^{b644} mutants (Fig 1A). BAC map position and sequence (CR848819, CR936374, AL844887, and BX649265) are available at http://zfin.org.

CRISPR/Cas9 mutagenesis

An optimal target site, 5′-GGGCACCCCTAAGGCTCCTG-3′, in the 5′ coding sequence of *pnrc2* was identified using the ZiFit Targeter software package (Sander et al, 2007; Sander et al, 2010). *pnrc2*-targeting gRNA (5′-CAGGAGCCTTAGGGGTGCCC-3′) and *Cas9* mRNA (Jao et al, 2013) were synthesized and co-injected into 1-cell stage embryos (135 ng and 200 ng, respectively) as described (Talbot and Amacher, 2014). At 24 hpf, a subset of injected embryos were individually screened by high-resolution melting analysis (HRMA) to assess target site mutation efficiency in somatic cells. Remaining embryos were raised and crossed to AB wild-type adults; F1 adults were screened for germline transmission of CRISPR-induced mutations using HRMA. HRMA revealed two unique *pnrc2* mutant alleles transmitted by an individual F0 founder at a transmission rate of ~13% (2 of 15 F1 individuals). We recovered one allele, *pnrc2*^{oz22}, and outcrossed *pnrc2*^{oz22} heterozygotes to the AB wild-type strain for two generations before intercrossing for phenotypic analyses. Primer sequences are listed in Table S4.

DNA extraction and pnrc2^{oz22} genotyping strategy

Individual embryos and adult fin tissue were lysed in 50 ul 1X ThermoPol Buffer (NEB) at 95°C for 10 minutes, digested at 55°C for 1–4 hours using 25–50 ug Proteinase K (BP1700, ThermoFisher), followed by Proteinase K inactivation at 95°C for 10 minutes. 1 ul of DNA extract was used as template in a standard 25 ul reaction with Taq polymerase according to manufacturer's protocol (NEB). To molecularly identify *pnrc2*^{oz22} carriers after PCR amplification, samples were digested with 20 units NsiI-HF (NEB) to distinguish cleavable wild-type from un-cleavable mutant amplicons. Reaction products were analyzed on a 2% agarose gel stained with Gel Red (Biotium). Primer sequences are listed in Table S4.

Morpholino injection

The *pnrc2* splice-blocking morpholino (sbMO) sequence is: 5′-ACTGGATGTCACctagcagaagaca-3′ (uppercase, sequence complementary to exon 3; lower case, sequence complementary to intron 2) (Gene Tools, LLC). The *upf1* sbMO, 5′-TTTTGGGAGTTTATACCTGGTTGTC-3′, was published previously (Wittkopp et al, 2009). The *rbfox1l* sbMO, 5′-GCATTTGTTTTACCCCAAACATCTG-3′, and *rbfox2* sbMO, 5′-TATAATGCTTTATATACCCCGAACA-3′, was published previously (Gallagher et al, 2011; Berberoglu et al, 2017). Morpholinos were diluted to 0.1–2 ng/nl in 0.2M KCl and 0.1% phenol red and injected into the yolk of 1-cell stage embryos. *pnrc2* sbMO dose was optimized by determining the highest dose that gave reproducible and rescuable phenotypic defects with no toxicity. Primers used to assess efficacy of *pnrc2* sbMO injection (Fig S1K–L) are listed in Table S4. *upf1, rbfox1l*, and *rbfox2* sbMO doses were performed according to published methods using doses that gave reproducible phenotypic defects matching published results (Wittkopp et al, 2009; Gallagher et al, 2011; Berberoglu et al, 2017). Embryos were incubated at 28.5°C until 6 hours post fertilization (hpf) and then transferred to 25°C thereafter, except for a subset of *rbfox1l/rbfox2* double-injected and uninjected control embryos that were incubated at 28.5°C until 24 hpf and subsequently scored for ability to move.

mRNA injection

Full length *pnrc2* cDNA was amplified by RT-PCR and subcloned into expression vector pCS2+ (Rupp et al, 1994; Turner and Weintraub, 1994) to generate plasmid *SP6-pnrc2-cDNA* (TLG109). For rescue experiments, *pnrc2* mRNA was synthesized using the SP6 mMessage Machine Kit (Life Technologies), diluted in 0.2M KCl with 0.1% phenol red, and injected into 1-cell stage embryos (150–600 pg mRNA per embryo). Primer sequences are listed in Table S4.

In situ hybridization

Whole mount in situ hybridization was performed as previously described (Broadbent and Read 1999; Jowett 1999) using DIG-labeled antisense probes. The full length *pnrc2* cDNA was amplified by RT-PCR and subcloned into pBSKS+ (Stratagene), linearized with BamHI, and transcribed using T7 RNA polymerase to make DIG-labeled antisense *pnrc2* riboprobe (Roche Life Science). The same construct was linearized with XhoI and transcribed using T3 RNA polymerase to make DIG-labeled sense *pnrc2* riboprobe. Riboprobes for *her1, her7, dlc, dld*, and *Venus* were made as previously described (Dill et al, 2005; Delaune et al, 2012). In situ hybridization chain reaction (HCR-ISH) was performed using a combination of five anti-sense 50-nt probes spanning the *her1* transcript according to published procedures (Choi et al, 2010; Choi et al, 2014) and a zebrafish-specific protocol provided by Molecular Instruments. Probe targeting sequences (5′ to 3′) were:

1. GGGTTTTGAAGTCGCGAATCTAAAGTATTATCCAGAAGAAGCGTTCGCAG,

2. CGCCTTGATCTCTCGCAGTCGCGGTTTTAGTCCTAATATACTCAACAGCC,
3. GAGAATGGAGGAGAGCTGCTTGAAAAGCCTGGAGACGGCGGAGGAGAAAT,
4. TCACCTGAAGATGAGGTCCTGGGACGACCGGTAATGAAGTCGTTGAGAGA, and
5. TCGTCTCAGAGTCCGTGGTTGAGAGGATTGAACAGAGCCACTAAACCGCA.

RNA analysis

Whole embryos (n=20 per time point or condition) were solubilized in Trizol for RNA extraction (Life Technologies). 1 ug total RNA was purified and reverse transcribed into cDNA with random primers and Superscript III reverse transcriptase (RT) according to the manufacturer's instructions (Life Technologies). Expression analysis of *pnrc2* using primer pairs spanning constitutive exons 2 and 3 were used for RT-PCR-based detection of *pnrc2* transcript (Fig 4G, S1K and Table S4 for primer sequences). Splicing of *pnrc2* using primer pairs spanning within and across each of three constitutive exons of the 3146 nt *pnrc2* mRNA were used for RT-PCR-based detection of spliced and unspliced *pnrc2* transcript (Fig S1K–L and Table S4 for primer sequences).

Plasmid construction and Transgenesis

The heat-shock reporter *hsp70l:Venus-her1* 3′UTR was assembled by PCR amplification and restriction digestion of the *hsp70l* promoter from Tol2kit construct #222 (entry plasmid *p5E-hsp70l)* (Kwan et al, 2007), in parallel with restriction digestion of the *Venus-her1* 3′UTR sequence from the *her1:her1-Venus* plasmid (Delaune et al, 2012), followed by ligation of both fragments into a modified version of pBSKS+ plasmid containing flanking I-SceI meganuclease recognition sites (Thermes et al, 2002). The *Venus-her1* 3′UTR fragment isolated from plasmid *her1:her1-Venus* contains the *Venus* coding sequence followed by 1.1 kb of *her1* 3′ noncoding sequence that includes the annotated 724 nt *her1* 3′UTR and native *her1* pA signal sequence (Delaune et al, 2012). Constructs were sequence confirmed; primers used for cloning are listed in Table S4. Transgenic lines were generated as previously described using I-SceI-based transgenesis (Thermes et al, 2002).

Stably transgenic heatshock assay

Adult fish carrying the stable *hsp70l:Venus-her1* 3′UTR transgene that transmits as a single Mendelian locus were crossed to AB wild-type fish and resulting progeny were either injected at the 1-cell stage with 6 ng splice-blocking *pnrc2* morpholino (sbMO) or were set aside as uninjected control siblings. Progeny were raised to mid-segmentation, heat-shocked at 37°C for 15 minutes, and fixed in 4% PFA at 0, 20, and 30 minutes post-heat-shock and processed for *Venus* in situ hybridization.

Immunohistochemistry

All embryos described below were immunostained following standard protocols using 4% PFA fixation, dehydration and rehydration in a methanol series, and incubation in blocking solution for 1 hour. Tg(*her1:her1-Venus*)^{bk15} embryos were immunostained in 2% BSA/2% goat serum/1% DMSO/0.1% Tween-20/PBS blocking solution with 1:1000 dilution chicken anti-GFP that recognizes Venus protein (A10262, Life Technologies), and 1:400 dilution goat anti-chicken Alexa-Fluor-488 (A11039, ThermoFisher). Mid-segmentation embryos from wild-type and *pnrc2*^{oz22} crosses were immunostained in 2% BSA/5% goat serum/0.1% Tween-20/PBS blocking solution with 1:200 dilution anti-zdc2 that recognizes DeltaC protein (ab73336, Abcam) according to previously published methods (Giudicelli et al, 2007) or immunostained in 2% BSA/10% goat serum/0.5% Triton X-100/PBS blocking solution with 1:100 anti-zdd2 that recognizes Dld protein according to previously published methods (Wright et al, 2011) (ab73331, Abcam), followed by 1:800 dilution goat anti-mouse Alexa-Fluor-488 (A11001, ThermoFisher). Nuclear counter-staining was performed by transferring and mounting dissected in situ-hybridized embryos from 80% glycerol into SlowFade Gold Antifade Mountant with DAPI (S36939, Thermo Fisher) and incubation at 4°C overnight prior to imaging.

Microscopy and Imaging

In situ hybridized embryos were mounted in Permount and imaged using an Axiocam HRc digital camera with AxioPlan2 microscope (Zeiss). Immunofluorescent embryos were dissected and flat mounted or whole mounted in 80% glycerol and imaged at 10x, 20x, and 60x magnification using MetaMorph software (Molecular Devices) on an Andor™ SpinningDisc Confocal Microscope (Oxford Instruments) with iXon Ultra EMCCD and Nikon Neo cameras; laser wavelength and intensity were set at 488 nm and 100% for Venus protein detection, 488 nm and 50% for Dlc protein detection, 488 nm and 100% for Dld protein detection, 561 nm and 30% for *her1* mRNA detection, 405 nm and 40% for DAPI detection, respectively, and bit depth at 16-bit. Maximum intensity projections using MetaMorph software are shown for Venus, Dlc, and Dld protein detection (Fig 7D–E, K–N). Single z-sections are shown for *her1* HCR-ISH and DAPI (Fig 7C–C′, F–F′; Fig S6A–B‴).

RESULTS

tortuga^{b644} is a Chromosome 16 deficiency allele

The *tortuga*^{b644} allele is an ENU-induced deletion that leads to the post-transcriptional accumulation of segmentation clock transcripts (Dill et al, 2005). Using genetic markers that distinguish wild-type AB and SJD mapping strains, we found that *b644* is a deficiency that maps to a 1.46 Mb region on Chromosome 16 spanning an interval of at least 20 known or predicted protein-coding RefSeq-annotated genes in genome assembly GRCz10/danRer10 (Howe et al, 2013). Haploid-based mapping revealed that the *tortuga* lesion lies 0.30 cM to the left and 0.37 cM to the right of the SSLP markers z13511 and z9511, respectively (Fig 1A). Using PCR-amplification of genomic regions (mostly in protein-coding genes) that lie between the two SSLP markers, we characterized the extent of the deletion in diploid embryos derived from heterozygous *b644* intercrosses by identifying genes that fail to amplify in *tortuga* homozygous mutant versus wild-type sibling embryos (Fig 1B). To better map deletion breakpoints, we analyzed presence or absence of amplicons near the presumptive ends of the *tortuga* deletion region of Chromosome 16. At the end near z13511, an intergenic region located ~124 kb upstream of *pou3f2b* failed to amplify, indicating the break lies in a ~206 kb interval between *mms22l* and the intergenic region (Fig 1B). Similar analysis at the other end indicates that the other breakpoint lies in the ~2.9 kb genomic interval between exon 1 and intron 3 of *snip1* (Fig 1B).

Injection of a BAC that includes pnrc2 rescues the her1 expression defect in tortuga mutants

To narrow the list of relevant candidate gene(s) in the *tortuga* deficiency, we injected four BACs spanning regions of the deletion interval between *pou3f2b* to *snip1* into zebrafish embryos at the 1-cell stage and assessed *her1* expression phenotype. Because *tortuga* mutants do not survive beyond larval stages, BACs were injected into embryos from a heterozygous intercross, from which ~25% are homozygous for the *tor* deletion. Injection of zebrafish BAC clone AL844887 spanning nine full-length open reading frames rescues the *her1* expression defect in *tor* mutants in a dose-dependent manner (Fig 1A, Fig S1A–D; Table S1).

Loss of pnrc2 is associated with accumulation of her1 mRNA in tortuga mutants

To identify the gene or genes on BAC AL844887 that restore proper *her1* expression in *tortuga* mutants, we first analyzed candidate gene expression by RT-PCR before and during segmentation. Of nine candidates present on BAC AL844887, only seven are expressed at relevant time points (Fig S1E; data not shown for *me1*). Of these seven, only *pnrc2*, *rragca*, and to a lesser extent, *akirin1*, are detectably expressed from BAC AL844887 when injected into *tortuga*^{b644} mutants (Fig S1F). We injected antisense morpholinos (MOs) into 1-cell stage wild-type embryos to determine whether knockdown of any of the three candidates recapitulated the *tor*-like *her1* expression defect. Injection of translation-blocking MOs targeting *akirin1* and *rragca* does not cause overt morphological or *her1* expression defects (Fig S1I–J), and injection of maximal non-toxic doses of *akirin1* or *rragca* mRNA into *tortuga* mutants does not rescue *her1* expression defects (data not shown). In contrast, injection of *pnrc2* splice-blocking MOs (sbMOs), that effectively disrupt proper *pnrc2* splicing (Fig S1K–L), disrupts *her1* expression just as in *tortuga*^{b644} mutants (Fig 1C–D). Injection of a second *pnrc2*-targeting translation-blocking MO gave the same phenotype (Fig S1H; see Methods). Importantly, co-injection of MO-resistant *pnrc2* mRNA with *pnrc2* sbMO restores normal *her1* expression (Fig 1C–E; Table 1).

Pnrc2 restores proper her1 expression in tortuga mutants

To determine whether Pnrc2 can also restore normal *her1* expression in *tortuga* mutants, we injected *pnrc2* mRNA into embryos from a *tor*^{b644} heterozygote intercross. To discriminate "rescued" *tor* mutants and wild-type siblings among injected intercross progeny, we developed a visual assay to unambiguously identify fish homozygous for the *tor* deletion. The *pou3f1* gene lies within the *tortuga* deletion (Fig 1A) and thus is not expressed in *tor*^{b644} mutant embryos, whereas in wild-type siblings, *pou3f1* mRNA is expressed anteriorly in a pattern easily distinguished from that of *her1* mRNA expression. By co-hybridizing *pou3f1* and *her1* antisense probes, *tor*^{b644} mutants are readily identified and assessed for rescue of *her1* expression. Using this assay, we find that *pnrc2* mRNA-injected *tortuga* mutants exhibit wild-type *her1* expression (Fig 2A–D′; Table 2), indicating that Pnrc2 can restore proper *her1* expression in *tor* mutants.

Targeted mutation of pnrc2 recapitulates the cyclic transcript accumulation phenotype of tor^{b644} mutants

Because the tor^{b644} allele is a multi-gene deficiency, we used CRISPR/Cas9 mutagenesis (Hruscha et al, 2013; Hwang et al, 2013; Talbot and Amacher, 2014) to generate a nonsense *pnrc2* allele. We isolated a 17 bp deletion allele, $pnrc2^{oz22}$ that causes an early frame shift and likely results in a truncated Pnrc2 protein. Compared to wild-type Pnrc2 (148 amino acids), the predicted mutant protein determined from sequenced genomic DNA contains the N-terminal 35 amino acids followed by 11 aberrant residues (Fig 2E), terminating well before the two highly conserved SH3 and NR box regions (Fig 1F). To determine whether the $pnrc2^{oz22}$ frame-shifting allele fails to complement the tor^{b644} deletion allele, we crossed $pnrc2^{oz22}$ and tor^{b644} heterozygotes and found that all $pnrc2^{oz22}/tor^{b644}$ trans-heterozygote progeny display the tor^{b644} *her1* expression defect (Fig 2F–G). As expected, homozygous $pnrc2^{oz22}$ mutants phenocopy the tor^{b644} *her1* expression defect (Fig 2H–H′). Additionally, expression of segmentation clock-associated *her7*, *dlc*, and *dld* transcripts is also abnormal in $pnrc2^{oz22}$ mutants (Fig 3) and in the cases of *her1* and *dlc*, arise due to post-transcriptional accumulation of mRNA (Fig S2), all consistent with previous observations in tor^{b644} mutants using intronic and exonic in situ probes that distinguish nascent from processed transcripts (Dill et al, 2005). Unlike tor^{b644} mutants, $pnrc2^{oz22}$ mutants and $pnrc2^{oz22}/tor^{b644}$ trans-heterozygotes do not have neural degeneration and somite shape defects, suggesting these *tor* mutant phenotypes are caused by loss of function of another gene or genes in the *tor* deletion interval. $pnrc2^{oz22/oz22}$ embryos appear morphologically normal and survive through 6 days post fertilization, but very few survive to adulthood (data not shown). Reduced survivorship of zebrafish $pnrc2^{oz22/oz22}$ mutants contrasts with Pnrc2-null mice that survive to adulthood and are indistinguishable from wild-type littermates up to 12 months of age (Zhou et al, 2008).

pnrc2 is broadly expressed during segmentation

To characterize embryonic *pnrc2* expression, we performed whole mount in situ hybridization and found that *pnrc2* is broadly expressed, with slight enrichment in somites and neural tissue during segmentation stages (Fig 4A–F). RT-PCR analysis of mRNA extracted from wild-type embryos confirms that *pnrc2* is expressed across similar stages examined by in situ (Fig 4G). Expression at the 8-cell stage (Fig 1A) and at the 1- and 2-cell stages (data not shown) suggests that *pnrc2* transcripts are maternally provided.

The her1 3′UTR confers instability to transcripts in a Pnrc2-dependent manner

In previous studies, heat-shock-induced reporter transcripts containing *her1* or *her7* coding and 3′UTR sequences decayed rapidly post-induction (Giudicelli et al, 2007). Because 3′UTR sequences can influence mRNA stability (Ghosh and Jacobson, 2010; Chen and Shyu, 2011; Schoenberg and Maquat, 2012), we hypothesized that the *her1* 3′UTR alone might be sufficient to trigger Pnrc2-mediated decay. We therefore developed a stable transgenic heat-shock reporter line to drive expression of a *Venus* transcript followed by the *her1* 3′UTR. We compared reporter expression after heat-shock of uninjected and *pnrc2* sbMO-injected *hsp70l:Venus-her1* 3′UTR transgenic siblings across multiple time points. Heat-shock-induced *Venus* transcripts are almost completely absent by 30 minutes post heat-shock (pHS) in the reporter line (Fig 5A–C). However, injection of *pnrc2* sbMO into *hsp70l:Venus-her1* 3′UTR embryos negates the destabilizing effect of the *her1* 3'UTR (Fig 5D–F; Table 3). These results support our hypothesis that Pnrc2-mediated decay of *her1* transcripts occurs through destabilizing features of the *her1* 3′UTR.

her1 expression is unaffected in embryos lacking maternal and zygotic Dicer function

It is well established that microRNAs (miRNAs) play an essential role in post-transcriptional gene regulation in developing zebrafish embryos (Bazzini et al, 2012; Giraldez, 2010; Giraldez et al, 2005; Mishima and Tomari, 2016; Mishima et al, 2006; Jonas and Izaurralde, 2015). Using TargetScan Fish (Ulitsky et al, 2012), we find that predicted miRNA target sites are present throughout the *her1* 3′UTR and other cyclic transcript 3′UTRs (Table S2). The 3′UTRs of *her1*, *her7*, *dlc*, and *dld* lack a common predicted target site, however some target sites are present in at least two of the four 3′UTRs analyzed. We therefore reasoned that miRNAs might influence the decay of *her1* and other transcripts. Using maternal-zygotic *dicer* (*MZdicer*) mutants that lack Dicer-dependent miRNA processing (Giraldez et al, 2005), we find that segmenting *MZdicer* mutants, despite having severe morphogenesis defects (Giraldez et al, 2005), have a normal striped *her1* expression pattern (n=11/11), demonstrating that proper *her1* expression is independent of Dicer-dependent miRNA function (Fig 5G–H).

Pnrc2 and Upf1 may genetically interact to promote her1 transcript decay

Human PNRC2 binds directly to nonsense-mediated decay (NMD) factors, including UPF1, and these interactions are required for decay of reporter mRNA in cultured cells (Cho et al, 2009; Lai et al, 2012). We therefore predicted that Pnrc2 and Upf1 might also interact to promote decay of non-aberrant, cyclic transcripts during segmentation. To determine whether Pnrc2 and Upf1 cooperatively regulate cyclic mRNA decay, we co-injected MOs targeting both transcripts and examined *her1* expression. As expected, injection of *pnrc2* sbMO at the optimal dose ("moderate", 6 ng) causes strong *her1* misexpression, but has no effect at a sub-optimal ("low") dose (2 ng) (Fig 6A–C). Strikingly, co-injection of a sub-optimal dose of *pnrc2* sbMO (2 ng) with a sub-optimal dose of *upf1* sbMO (0.25 ng) results in a *her1* expression defect markedly similar to that observed with optimal doses of *pnrc2* sbMO alone (6 ng) (Fig 6B–E, quantified in F). Interestingly, single *upf1* knockdown at published (0.65 ng) or higher doses (2 ng) does not alter *her1* mRNA expression, but does induce the expected published phenotypes including neural necrosis and abnormal segment formation (data not shown) (Wittkopp et al, 2009; Anastasaki et al, 2011). As a control, we injected a sub-optimal dose of *pnrc2* sbMO (2 ng) with an unrelated MO, *rbfox1l* sbMO, at the published 6 ng dose (Gallagher et al, 2011; Berberoglu et al, 2017), and observed that *her1* mRNA expression is normal (Fig S3), suggesting that *her1* misexpression in embryos co-injected with sub-optimal doses of *pnrc2* and *upf1* sbMOs is a specific effect. Taken together, these results reveal that depletion of Upf1 sensitizes embryos to partial loss of Pnrc2. Although depletion of Upf1 alone does not affect *her1* expression, it is possible that low levels of Upf1 protein persist in *upf1* morphants and may be sufficient for cyclic mRNA clearance in the presence of normal levels of Pnrc2.

Unlike mRNAs, cyclic proteins do not accumulate upon Pnrc2 depletion

Our data indicate that Pnrc2 triggers decay of reporter mRNAs and natural cyclic transcripts like *her1*. Previous work has shown that embryos injected with *her1* mRNA at the 1-cell stage have severe somite patterning and boundary defects, as well as decreased expression of Her1 transcriptional targets like *dlc* and *her7* (Takke and Campos-Ortega, 1999; Giudicelli et al, 2007). The morphological phenotype of embryos constitutively overexpressing *her1* contrasts sharply with that of *pnrc2*^{oz22} mutant embryos, which have normal somite numbers and boundaries (Table 4 and data not shown) despite dramatic accumulation of endogenous *her1* and other cyclic transcripts. We therefore hypothesized that accumulated *her1* transcripts in *pnrc2*^{oz22} mutants do not result in increased Her1 protein. Because a Her1 antibody is lacking, we tested this idea by depleting *pnrc2* function in a validated transgenic cyclic reporter line, *Tg(her1:her1-Venus)*^{pk15}, that infers *her1* transcript and Her1 protein dynamics via detection of *her1-Venus* reporter mRNA and protein (Delaune et al, 2012; Shih et al, 2015). As expected, *her1-Venus* transcripts are misexpressed in *pnrc2* morphants carrying the cyclic reporter transgene, mirroring what is observed for endogenous *her1* transcripts (Fig 7A–B). Her1-Venus reporter protein expression, however, is indistinguishable between uninjected and *pnrc2* sbMO-injected transgenic embryos (Fig 7D–E). Her1-Venus protein expression is similarly unaffected in transgenic reporter embryos injected with sub-optimal doses of *pnrc2* sbMO (2 ng) and *upf1* sbMO (0.25 ng) as well as transgenic reporter embryos co-injected with an optimal dose of *pnrc2* sbMO (6 ng) together with a higher dose of *upf1* sbMO (2 ng) (Fig S4; Table S3). Together, the observed misexpression of *her1-Venus* mRNA, but not Her1-Venus protein, is consistent with our hypothesis that *pnrc2* mutants segment normally because accumulated *her1* transcripts do not result in abnormal levels of Her1 protein.

Discordant transcript and protein expression in *pnrc2* mutants and morphants might be due to nuclear retention of accumulated mRNA, so we employed in situ hybridization chain reaction (HCR-ISH) (Choi et al, 2010; Choi et al, 2014) coupled with DAPI nuclear counter staining to assess sub-cellular localization of *her1* mRNA. As a control for probe set specificity, we first performed *her1* HCR-ISH on wild-type and *Df(Chr05:her1,her7,ndrg3a)*^{b567} homozygote embryos that lack the linked *her1* and *her7* genes (Henry et al, 2002) and find that *b567* homozygotes lack detectable signal (Fig S5). We then performed HCR-ISH on both wild-type and *pnrc2* mutants and find substantial cytoplasmic localization of *her1* mRNA in both conditions, suggesting that accumulated transcripts in *pnrc2* mutants are not retained in the nucleus and are properly exported to the cytoplasm (Fig 7C–C′, F–F′; Fig S6A–A″, B–B″). Because relative intensity of *her1* HCR-ISH in *pnrc2* mutants to wild-type embryos is high, levels have been reduced in *pnrc2* mutant panels (Fig 7F–F′; Fig S6B–B″). Intensity maps of raw *her1* HCR-ISH signal reflect the extent of *her1* mRNA accumulation in *pnrc2*^{oz22} mutants (Fig S6A‴, B‴). Overall, despite the increase in *her1* mRNA levels, accumulated transcripts in *pnrc2* mutants are exported from the nucleus, consistent with our hypothesis that Pnrc2 promotes decay of cyclic mRNA, a process that likely employs cytoplasmic decay machinery (Garneau et al, 2007; Schoenberg and Maquat, 2012).

Having established that *her1-Venus* reporter mRNA, but not protein, is misexpressed in *pnrc2* morphants, we next asked whether discordant expression occurs for other cyclic transcripts and proteins. Siblings from a *pnrc2*^{oz22} heterozygote intercross were split and processed in parallel for mRNA and protein expression analysis. While *pnrc2*^{oz22} homozygous mutants were readily distinguished from unaffected siblings based on *dlc* and *dld* mRNA misexpression (Fig 7G–J), there were no discernible differences in Dlc and Dld protein expression among sibling embryos (Fig 7K–N). Overall, we provide evidence that despite the accumulation of cyclic transcripts in *pnrc2*^{oz22} mutants, cyclic protein expression is unaffected, which may help explain the absence of obvious segmentation phenotypes.

DISCUSSION

In this work, we present evidence that Pnrc2 promotes the decay of cyclic mRNAs and that the *her1* 3′UTR is sufficient to trigger Pnrc2-mediated decay. Our work builds upon previous studies of Pnrc2-regulated mRNA decay and reveals natural, developmentally-regulated transcripts that are targets of Pnrc2-mediated decay. Zebrafish Pnrc2 shares significant similarity with human PNRC2. Residues in human PNRC2 that are required for decay of reporter mRNA containing a premature termination codon (PTC) are conserved in zebrafish, and include K109 (K119 in zebrafish), W114 (W124 in zebrafish), and the C-terminal KTLLK nuclear receptor domain (NR box) (KSLLK in zebrafish) (Fig 1F) (Cho et al, 2009; Lai et al, 2012). PNRC2 does not bind mRNA directly in human cultured cells, but instead functions via interactions with decay factors SMG6, DCP1A, UPF1, and STAU1 to regulate decay of PTC-containing reporter transcript (Cho et al, 2009; Cho et al, 2012; Cho et al, 2013a; Cho et al, 2013b; Cho et al, 2015; Lai et al, 2012). Our work shows that in segmenting zebrafish embryos, *pnrc2* and *upf1* may also interact to promote decay of natural, developmentally-regulated transcripts. Future identification of factors that participate in the Pnrc2-mediated decay process will define this key aspect of oscillatory gene regulation and to what extent it employs existing, well-characterized RNA decay machinery.

Cyclic transcript accumulation is due to loss of Pnrc2 in tortuga and pnrc2 mutants

Because the *tor*^{b644} allele is a multi-gene deficiency, we generated a nonsense *pnrc2* allele. As expected, *pnrc2*^{oz22} mutants show misexpression of cyclic transcripts including the cyclic transcripts *her1*, *her7*, and *dlc*, as well as *dld* (Figs 2–3), and in the cases of *her1* and *dlc*, accumulate post-transcriptionally (Fig S2), all consistent with previous observations in *tor*^{b644} mutants (Dill et al, 2005). Because an early frame shift *pnrc2* mutation has the same impact on *her1* post-transcriptional regulation as complete deletion of the *pnrc*2 locus, it is unlikely that accumulation of *her1* transcripts is due to loss or mutation of miRNA- or lncRNA-encoding genes at or near the *pnrc2* locus, but is instead due to loss of Pnrc2 protein.

Pnrc2 translation may be developmentally regulated

pnrc2 transcripts are maternally provided and broadly expressed (Fig 4), however *pnrc2* may be subject to translational regulation. Using global ribosomal profiling experiments in developing zebrafish embryos, Giraldez and colleagues showed that the *pnrc2* transcript contains a conserved upstream open reading frame (uORF) that lies out of frame with the Pnrc2-coding ORF and is preferentially associated with translational machinery during early embryonic stages (Lee and Bonneau et al, 2013). The presence of two ORFs, an uORF and the Pnrc2-coding ORF, suggests that Pnrc2 translation may be affected by translation at the uORF, as has been demonstrated in other organisms and contexts (Gebauer and Hentze, 2004; Hood et al, 2009; Medenbach et al, 2011; Morris and Geballe, 2000; Sachs and Geballe, 2006; Somers et al, 2013; Wethmar 2014). An uORF can also act as an NMD-inducing feature (Barbosa et al, 2013; Peccarelli and Kebaara, 2014), adding another layer of possible post-transcriptional regulation. It is also interesting that transcripts encoding several NMD factors, like UPF2 and SMG factors, themselves contain uORFs that confer post-transcriptional regulation via feedback control (Popp and Maquat, 2013). Future development of antibodies for detection of zebrafish Pnrc2 and other decay factors will help to advance our understanding of Pnrc2-mediated decay in a developmental context.

Expression patterns of cyclic proteins appear normal despite accumulated cyclic transcripts in pnrc2-deficient embryos

It is remarkable that the dramatic accumulation of Pnrc2-regulated cyclic transcripts like *her1* in *tor* and *pnrc2* mutant embryos does not confer phenotypes typically associated with excess Her1, like somite boundary defects and down-regulation of Her1 transcriptional targets including *dlc* and *her7* (Takke and Campos-Ortega, 1999; Giudicelli et al, 2007). Similarly, accumulation of *dlc* transcripts in *tor* and *pnrc2* mutants does not confer somite boundary defects associated with excess Dlc protein (Soza-Ried, 2014). We find that *pnrc2* mutants lack such phenotypes and hypothesize that this is due to normal cyclic protein expression despite mRNA accumulation. It remains unclear why accumulated *her1* transcripts in *pnrc2* mutants fail to produce defects associated with excess Her1, particularly because previous *her1* overexpression experiments included the full length *her1* 3′UTR (Takke and Campos-Ortega, 1999; Giudicelli et al, 2007) that we now show confers Pnrc2-dependent instability. Overall, because Her1-Venus reporter protein and endogenous Dlc and Dld proteins are expressed normally despite misexpression of mRNA in *pnrc2*-deficient embryos (Fig 7; Fig S4; Table S3), we suggest that Pnrc2-mediated mRNA decay acts in addition to a regulatory layer that controls oscillatory protein expression. Although the *her1* transcript does not contain obvious NMD-inducing features such as an uORF and accumulated *her1* transcripts in *pnrc2* mutants do not appear retained in nuclei (Fig 7F′; Fig S6B″), there are other mechanisms that may function to repress or prevent translation (Mishima et al, 2012; Takeda et al, 2009; Yasuda et al, 2010; Takahashi et al, 2014; Subtelny et al, 2014; Mishima and Tomari, 2016). Alternatively, normal cyclic protein expression in *pnrc2* mutants might occur because protein decay machinery compensates for increased cyclic expression. Treatment of cultured mouse cells with ubiquitin-proteasome inhibitors stabilizes Hes1 protein (closely related to zebrafish Her1) (Hirata, 2002) and mathematical modeling predicts short half-lives for zebrafish Her1 and Her7 proteins (Lewis, 2003). More recently, it has been shown that translational fusion of Her1 to Venus reporter protein confers protein instability (Delaune et al, 2012) and measurements of Her7 protein half-life reveal rapid turnover of Her7 protein within 3.5 minutes (Ay et al, 2013). Future investigation into destabilizing features that trigger rapid protein decay might provide insight into the contribution of protein decay in maintaining oscillatory expression.

Potential cis-regulatory elements reside in the her1 3′UTR

Our data show that the *her1* 3′UTR is sufficient to trigger Pnrc2-dependent decay of reporter mRNA. It is well known that 3′UTR sequences can influence mRNA stability by length-dependent, sequence, and/or structural feature recognition (Ghosh and Jacobson, 2010; Chen and Shyu, 2011; Schoenberg and Maquat, 2012). We favor the latter two possibilities because the *her1* 3′UTR is of average length with respect to the post-gastrulation zebrafish transcriptome (Li et al, 2012; Ulitsky et al, 2012; Mishima and Tomari, 2016) and analysis of the *her1* 3′UTR using the mfold Web Server (Zuker, 2003) predicts a stable stem-loop structure (data not shown). Future biochemical methods of structure probing coupled with deletion reporter assays will help determine if mfold-predicted structures are functionally relevant.

mRNA decay pathways include AU-rich element (ARE)-mediated (von Roretz and Gallouzi, 2008), Staufen1 (Stau1)-mediated (Park and Maquat, 2013), nonsense-mediated (Schoenberg and Maquat, 2012), and miRNA-mediated (Bazzini et al, 2012; Giraldez, 2010; Mishima and Tomari, 2016; Mishima et al, 2006; Jonas and Izaurralde, 2015) decay. Normal *her1* expression in *MZdicer* mutants (Fig 5G–H) suggests that miRNA-mediated decay does not contribute to *her1* oscillatory expression despite the presence of numerous predicted miRNA 3′UTR sites (Table S2), although we have not ruled out the possibility that Dicer-independent miRNAs contribute to *her1* mRNA decay. Additional motif searches of the *her1* 3′UTR using AREsite2 (Fallmann et al, 2016) yield four ARE core motif ATTTA sequences in addition to numerous other ARE-related motifs for *her1* and other cyclic 3′UTRs that might promote mRNA decay (data not shown). Experiments using deletion reporter assays are underway that will functionally test the role of these and other potential regulatory elements.

We favor nonsense mediated decay (NMD) and/or Stau1-mediated decay (SMD), both of which are Upf1-dependent, as the most likely pathway(s) utilized to clear natural cyclic transcripts during segmentation. Upf1 and Pnrc2 promote decay of cyclic transcripts during segmentation (Fig 6; Fig S4; Table S3) and others have shown that human PNRC2 acts as a decay adapter that physically interacts with decay factors DCP1 and UPF1 and can promote decapping activity of Dcp2 *in vitro* (Cho et al, 2009; Cho et al, 2012; Cho et al, 2013a; Cho et al, 2013b; Cho et al, 2015; Lai et al, 2012; Mugridge et al, 2016). Transcripts annotated in zebrafish EST and GenBank databases (GRCv10) for *her1*, *dlc*, and *dld* lack canonical NMD-inducing features (retained introns, premature termination codons, upstream ORFs, or intron-containing 3′UTRs), although there exists an intron-retained *her7* isoform. Global analyses of UPF1-binding sites in murine embryonic stem cells (mESCs) uncovered a large class of UPF1-3′UTR-bound mRNAs that undergo repression by NMD despite lacking canonical NMD-inducing features, although cyclic transcripts were not among those analyzed (Hurt et al, 2013). Because *upf1* knockdown alone does not affect *her1* expression, but partial knockdown of *pnrc2* together with *upf1* leads to accumulated *her1* mRNA (Fig 6; Fig S4; Table S3 and data not shown), it is unlikely that Upf1 is absolutely required for Pnrc2-mediated decay of cyclic transcripts (although maternally-provided *upf1* function may mask such a function). Instead, it may be that Pnrc2 promotes decay through a combination of Upf1-dependent and -independent mechanisms. Alternatively, low levels of Upf1 protein may be sufficient for Pnrc2-mediated cyclic mRNA decay. Substantial depletion of Upf1 protein is achieved with splice-blocking morpholinos, however, Upf1 is faintly detected by immunoblot (Wittkopp et al, 2009) and this may be sufficient for cyclic mRNA clearance when Pnrc2 levels are normal. Future biochemical and genetic interaction studies with known factors of NMD and SMD will further enhance our understanding of mechanisms that drive rapid decay of cyclic transcripts during segmentation.

CONCLUSIONS

Overall, we propose that cyclic mRNA accumulation in *tortuga* and *pnrc2* mutants results from misregulation of 3′UTR-mediated mRNA decay. This decay process occurs independently of Dicer-generated miRNAs and instead employs decay machinery associated with nonsense-mediated decay. *pnrc2* mutants have normal segment number and this is likely due to normal expression of cyclic proteins despite misexpression of cyclic transcripts. Future biochemical, molecular, and genetic studies will provide a deeper understanding of the segmentation clock and post-transcriptional mechanisms that regulate oscillatory expression.

Supplementary Material

Refer to Web version on PubMed Central for supplementary material.

Acknowledgments

We thank UC Berkeley and Ohio State Zebrafish Facilities staff for excellent zebrafish care, Paula Monsma and the Neurobiology Imaging Core for microscopy assistance and advice, and the OSU Center for RNA Biology. We thank Jared Talbot for assistance with CRISPR-based mutagenesis, Kariena Dill and Jenny Lu for early work on *tortuga* mapping, Stephen Gross for computational identification of novel mapping markers, Antonio Giraldez, Carter Takacs, Valeria Yartseva, and Hiba Codore for advice and sharing of *MZ-dicer* embryos, Steven Brenner and Courtney French for advice and sharing unpublished data, Anne Witzky and Rachel Leist for experimental assistance, and Guramit Singh for advice and sharing equipment.

FUNDING

This work was supported by NIH grants GM061952 and GM117964 (S.L.A.), an OSU Center for RNA Biology Predoctoral Fellowship (K.T.T.), an NSF Predoctoral Fellowship (J.M.M.), and a UC Berkeley Haas Scholars Undergraduate Fellowship (M.L.G.).

References

Anastasaki C, Longman D, Capper A, Patton EE, Cáceres JF. Dhx34 and Nbas function in the NMD pathway and are required for embryonic development in zebrafish. Nucleic Acids Res. 2011; 39(9): 3686–3694. [PubMed: 21227923]

Ay A, Holland J, Sperlea A, Devakanmalai GS, Knierer S, Sangervasi S, Stevenson A, Özbudak EM. Spatial gradients of protein-level time delays set the pace of the traveling segmentation clock waves. Dev. 2014; 141:4158–4167.

Ay A, Knierer S, Sperlea A, Holland J, Özbudak EM. Short-lived Her proteins drive robust synchronized oscillations in the zebrafish segmentation clock. Dev. 2013; 140(15):3244–3253.

Barbosa C, Peixeiro I, Romão L. Gene expression regulation by upstream open reading frames and human disease. PLoS Genet. 2013; 9(8):e1003529. [PubMed: 23950723]

Bardwell V, Wickens M. Purification of RNA and RNA-protein complexes by R17coat protein affinity chromatography. Nucleic Acids Res. 1990; 18:6587–6594. [PubMed: 1701242]

Bazzini AA, Lee MT, Giraldez AJ. Ribosome profiling shows that *miR-430* reduces translation before causing mRNA decay in zebrafish. Science. 2012; 336(6078):233–237. [PubMed: 22422859]

Berberoglu MA, Gallagher TL, Morrow ZT, Talbot JC, Hromowyk KJ, Tenente IM, Langenau DM, Amacher SL. Satellite-like cells contribute to *pax7*-dependent skeletal muscle repair in adult zebrafish. Dev Biol. 2017; 424(2):162–180. [PubMed: 28279710]

Bessho Y, Hirata H, Masamizu Y, Kageyama R. Periodic repression by the bHLH factor Hes7 is an essential mechanism for the somite segmentation clock. Genes Dev. 2003; 17:1451–1456. [PubMed: 12783854]

Bessho Y, Sakata R, Komatsu S, Shiota K, Yamada S, Kageyama R. Dynamic expression and essential functions of Hes7 in somite segmentation. Genes Dev. 2001; 15:2642–2647. [PubMed: 11641270]

Bonev B, Stanley P, Papalopulu N. *MicroRNA-9* modulates *Hes1* ultradian oscillations by forming a double-negative feedback loop. Cell Rep. 2012; 2(1):10–18. [PubMed: 22840391]

Broadbent J, Read EM. Wholemount in situ hybridization of *Xenopus* and zebrafish embryos. Methods Mol Biol. 1999; 127:57–67. [PubMed: 10503224]

Chen CY, Shyu AB. Mechanisms of deadenylation-dependent decay. Wiley Interdiscip Rev RNA. 2011; 2(2):167–183. [PubMed: 21957004]

Cho H, Han S, Choe J, Park SG, Choi SS, Kim YK. SMG5-PNRC2 is functionally dominant compared with SMG5-SMG7 in mammalian nonsense-mediated mRNA decay. Nucleic Acids Res. 2013; 41(2):1319–1328. [PubMed: 23234702]

Cho H, Han S, Park OH, Kim YK. SMG1 regulates adipogenesis via targeting of Staufen1-mediated mRNA decay. Biochim Biophys Acta. 2013; 1829(12):1276–1287. *Erratum in*: (2014). *Biochim. Biophys. Acta* 1839(9), 898. [PubMed: 24185201]

Cho H, Kim KM, Kim YK. Human proline-rich nuclear receptor coregulatory protein 2 mediates an interaction between mRNA surveillance machinery and decapping complex. Mol Cell. 2009; 33:75–86. [PubMed: 19150429]

Cho H, Kim KM, Han S, Choe J, Park SG, Choi SS, Kim YK. Staufen1-mediated mRNA decay functions in adipogenesis. Mol Cell. 2012; 46:495–506. [PubMed: 22503102]

Cho H, Park OH, Park J, Ryu I, Kim J, Ko J, Kim YK. Glucocorticoid receptor interacts with PNRC2 in a ligand-dependent manner to recruit UPF1 for rapid mRNA degradation. Proc Natl Acad Sci USA. 2015; 112(13):E1540–9. [PubMed: 25775514]

Choi HM, Beck VA, Pierce NA. Next-generation in situ hybridization chain reaction: higher gain, lower cost, greater durability. ACS Nano. 2014; 8(5):4284–4294. [PubMed: 24712299]

Choi HM, Chang JY, Trinh le A, Padilla JE, Fraser SE, Pierce NA. Programmable in situ amplification for multiplexed imaging of mRNA expression. Nat Biotechnol. 2010; 28(11):1208–1212. [PubMed: 21037591]

Cibois M, Gautier-Courteille C, Legagneux V, Paillard L. Post-transcriptional controls – adding a new layer of regulation to clock gene expression. Trends Cell Biol. 2010; 20:533–541. [PubMed: 20630760]

Clement SL, Lykke-Andersen J. A tethering approach to study proteins that activate mRNA turnover in human cells. Methods Mol Biol. 2008; 419:121–133. [PubMed: 18369979]

Coller JM, Gray NK, Wickens MP. mRNA stabilization by poly(A) binding protein is independent of poly(A) and requires translation. Genes Dev. 1998; 12:3226–3235. [PubMed: 9784497]

Delaune EA, François P, Shih NP, Amacher SL. Single-cell-resolution imaging of the impact of Notch signaling and mitosis on segmentation clock dynamics. Dev Cell. 2012; 23(5):995–1005. [PubMed: 23153496]

Dill KK, Amacher SL. *tortuga* refines Notch pathway gene expression in the zebrafish presomitic mesoderm at the post-transcriptional level. Dev Biol. 2005; 287(2):225–236. [PubMed: 16236276]

Fallmann J, Sedlyarov V, Tanzer A, Kovarik P, Hofacker IL. AREsite2: an enhanced database for the comprehensive investigation of AU/GU/U-rich elements. Nucleic Acids Res. 2016; 44(D1):D90–5. [PubMed: 26602692]

Fürthauer M, Thisse C, Thisse B. A role for FGF-8 in the dorsoventral patterning of the zebrafish gastrula. Dev. 1997; 124(21):4253–4264.

Fujimuro T, Matsui T, Nitanda Y, Matta T, Sakumura Y, Saito M, Kohno K, Nakahata Y, Bessho Y. *Hes7* 3′UTR is required for somite segmentation function. Sci Rep. 2014; 4:6462. [PubMed: 25248974]

Gajewski M, Sieger D, Alt B, Leve C, Hans S, Wolff C, Rohr KB, Tautz D. Anterior and posterior waves of cyclic *her1* gene expression are differentially regulated in the presomitic mesoderm of zebrafish. Dev. 2003; 130(18):4269–4278.

Gallagher TL, Arribere JA, Geurts PA, Exner CR, McDonald KL, Dill KK, Marr HL, Adkar SS, Garnett AT, Amacher SL, Conboy JG. Rbfox-regulated alternative splicing is critical for zebrafish cardiac and skeletal muscle functions. Dev Biol. 2011; 359(2):251–261. [PubMed: 21925157]

Garneau NL, Wilusz J, Wilusz CJ. The highways and byways of mRNA decay. Nat Rev Mol Cell Biol. 2007; 8(2):113–126. [PubMed: 17245413]

Gebauer F, Hentze MW. Molecular mechanisms of translational control. Nat Rev Mol Cell Biol. 2004; 5:827–835. [PubMed: 15459663]

Ghosh S, Jacobson A. RNA decay modulates gene expression and controls its fidelity. Wiley Interdiscip Rev RNA. 2010; 1(3):351–361. [PubMed: 21132108]

Giraldez AJ. microRNAs, the cell′s Nepenthe: clearing the past during the maternal-to-zygotic transition and cellular reprogramming. Curr Opin Genet Dev. 2010; 20(4):369–375. [PubMed: 20452200]

Giraldez AJ, Cinalli RM, Glasner ME, Enright AJ, Thomson JM, Baskerville S, Hammond SM, Bartel DP, Schier AF. MicroRNAs regulate brain morphogenesis in zebrafish. Science. 2005; 308(5723): 833–8. [PubMed: 15774722]

Giudicelli F, Ozbudak EM, Wright GJ, Lewis J. Setting the tempo in development: an investigation of the zebrafish somite clock mechanism. PLoS Biol. 2007; 5(6):e150. [PubMed: 17535112]

González A, Manosalva I, Liu T, Kageyama R. Control of *Hes7* expression by Tbx6, the Wnt pathway and the chemical Gsk3 inhibitor LiCl in the mouse segmentation clock. PLoS One. 2013; 8(1):e53323. [PubMed: 23326414]

Graveley BR, Maniatis T. Arginine/serine-rich domains of SR proteins can function as activators of pre-mRNA splicing. Mol Cell. 1998; 1(5):765–771. [PubMed: 9660960]

Hanisch A, Holder MV, Choorapoikayil S, Gajewski M, Ozbudak EM, Lewis J. The elongation rate of RNA polymerase II in zebrafish and its significance in the somite segmentation clock. Dev. 2013; 140(2):444–453.

Harima Y, Imayoshi I, Shimojo H, Kobayashi T, Kageyama R. The roles and mechanism of ultradian oscillatory expression of the mouse *Hes genes*. Semin Cell Dev Biol. 2014; (34):85–90.

Harima Y, Takashima Y, Ueda Y, Ohtsuka T, Kageyama R. Accelerating the tempo of the segmentation clock by reducing the number of introns in the *Hes7* gene. Cell Rep. 2013; 3(1):1–7. [PubMed: 23219549]

Henry CA, Urban MK, Dill KK, Merlie JP, Page MF, Kimmel CB, Amacher SL. Two linked *hairy/Enhancer of split-related* zebrafish genes, *her1* and *her7*, function together to refine alternating somite boundaries. Dev. 2002; 129:3693–3704.

Hentschke M, Borgmeyer U. Identification of PNRC2 and TLE1 as activation function-1 cofactors of the orphan nuclear receptor ERRE. Biochem Biophys Res Commun. 2003; 312(4):975–982. [PubMed: 14651967]

Heyn P, Kircher M, Dahl A, Kelso J, Tomancak P, Kalinka AT, Neugebauer KM. The earliest transcribed zygotic genes are short, newly evolved, and different across species. Cell Rep. 2014; 6(2):285–292. [PubMed: 24440719]

Hilgers V, Pourquié O, Dubrulle J. *In vivo* analysis of mRNA stability using the Tet-Off system in the chicken embryo. Dev Biol. 2005; 284(2):292–300. [PubMed: 15993405]

Hirata H, Yoshiura S, Ohtsuka T, Bessho Y, Harada T, Yoshikawa K, Kageyama R. Oscillatory expression of the bHLH factor Hes1 regulated by a negative feedback loop. Science. 2002; 298:840–843. [PubMed: 12399594]

Holley SA, Geisler R, Nüsslein-Volhard C. Control of *her1* expression during zebrafish somitogenesis by a *Delta*-dependent oscillator and an independent wave-front activity. Genes Dev. 2000; 14(13): 1678–1690. [PubMed: 10887161]

Hood HM, Neafsey DE, Galagan J, Sachs MS. Evolutionary roles of upstream open reading frames in mediating gene regulation in fungi. Annu Rev Microbiol. 2009; 63:385–409. [PubMed: 19514854]

Horton RM, Cai ZL, Ho SN, Pease LR. Gene splicing by overlap extension: tailor-made genes using the polymerase chain reaction. Biotechniques. 1990; 8:528–535. [PubMed: 2357375]

Houseley J, Tollervey D. The many pathways of RNA degradation. Cell. 2009; 136(4):763–776. [PubMed: 19239894]

Howe K, Clark MD, Torroja CF, Torrance J, Berthelot C, Muffato M, Collins JE, Humphray S, McLaren K, Matthews L, et al. The zebrafish reference genome sequence and its relationship to the human genome. Nature. 2013; 496(7446):498–503. [PubMed: 23594743]

Hoyle NP, Ish-Horowicz D. Transcript processing and export kinetics are rate-limiting steps in expressing vertebrate segmentation clock genes. Proc Natl Acad Sci USA. 2013; 110(46):E4316–4324. [PubMed: 24151332]

Hruscha A, Krawitz P, Rechenberg A, Heinrich V, Hecht J, Haass C, Schmid B. Efficient CRISPR/Cas9 genome editing with low off-target effects in zebrafish. Dev. 2013; 140(24):4982–4987.

Hubaud A, Pourquié O. Signalling dynamics in vertebrate segmentation. Nat Rev Mol Cell Biol. 2014; 15(11):709–721. [PubMed: 25335437]

Hurt JA, Robertson AD, Burge CB. Global analyses of UPF1 binding and function reveal expanded scope of nonsense-mediated mRNA decay. Genome Research. 2013; 23(10):1636–1650. [PubMed: 23766421]

Hwang WY, Fu Y, Reyon D, Maeder ML, Tsai SQ, Sander JD, Peterson RT, Yeh JR, Joung JK. Efficient genome editing in zebrafish using a CRISPR-Cas system. Nat Biotechnol. 2013; 31:227–229. [PubMed: 23360964]

Jao LE, Wente SR, Chen W. Efficient multiplex biallelic zebrafish genome editing using a CRISPR nuclease system. Proc Natl Acad Sci USA. 2013; 110(34):13904–13909. [PubMed: 23918387]

Jonas S, Izaurralde E. Towards a molecular understanding of microRNA-mediated gene silencing. Nat Rev Genet. 2015; 16(7):421–33. [PubMed: 26077373]

Jowett T. Analysis of protein and gene expression. Methods Cell Biol. 1999; 59:63–85. [PubMed: 9891356]

Kim YK, Furic L, Desgroseillers L, Maquat LE. Mammalian Staufen1 recruits Upf1 to specific mRNA 3′UTRs so as to elicit mRNA decay. Cell. 2005; 120:195–208. [PubMed: 15680326]

Kimmel CB, Ballard WW, Kimmel SR, Ullmann B, Schilling TF. Stages of embryonic development of the zebrafish. Dev Dyn. 1995; 203(3):253–310. [PubMed: 8589427]

Kwan KM, Fujimoto E, Grabher C, Mangum BD, Hardy ME, Campbell DS, Parant JM, Yost HJ, Kanki JP, Chien CB. The Tol2kit: a multisite gateway-based construction kit for Tol2 transposon transgenesis constructs. Dev Dyn. 2007; 236(11):3088–3099. [PubMed: 17937395]

Lai T, Cho H, Liu Z, Bowler MW, Piao S, Parker R, Kim YK, Song H. Structural basis of the PNRC2-mediated link between mRNA surveillance and decapping. Structure. 2012; 20:2025–2037. [PubMed: 23085078]

Lee MT, Bonneau AR, Takacs CM, Bazzini AA, DiVito KR, Fleming ES, Giraldez AJ. Nanog, Pou5f1 and SoxB1 activate zygotic gene expression during the maternal-to-zygotic transition. Nature. 2013; 503(7476):360–364. [PubMed: 24056933]

Levine JH, Lin Y, Elowitz MB. Functional Roles of Pulsing in Genetic Circuits. Science. 2013; 342(6163):1193–2000. [PubMed: 24311681]

Lewis J. Autoinhibition with transcriptional delay: A simple mechanism for the zebrafish somitogenesis oscillator. Curr Biol. 2003; 13:1398–1408. [PubMed: 12932323]

Link V, Shevchenko A, Heisenberg CP. Proteomics of early zebrafish embryos. BMC Dev Biol. 2006; 6:1. [PubMed: 16412219]

Li Y, Sun Y, Fu Y, Li M, Huang G, Zhang C, Liang J, Huang S, Shen G, Yuan S, Chen L, Chen S, Xu A. Dynamic landscape of tandem 3′ UTRs during zebrafish development. Genome Res. 2012; 22(10):1899–1906. [PubMed: 22955139]

Lykke-Andersen S, Jensen TH. Nonsense-mediated mRNA decay: an intricate machinery that shapes transcriptomes. Nat Rev Mol Cell Biol. 2015; 16(11):665–77. [PubMed: 26397022]

Medenbach J, Seiler M, Hentze MW. Translational control via protein-regulated upstream open reading frames. Cell. 2011; 145:902–913. [PubMed: 21663794]

Mishima Y, Fukao A, Kishimoto T, Sakamoto H, Fujiwara T, Inoue K. Translational inhibition by deadenylation-independent mechanisms is central to microRNA-mediated silencing in zebrafish. Proc Natl Acad Sci USA. 2012; 109(4):1104–1109. [PubMed: 22232654]

Mishima Y, Giraldez AJ, Takeda Y, Fujiwara T, Sakamoto H, Schier AF, Inoue K. Differential regulation of germline mRNAs in soma and germ cells by zebrafish miR-430. Curr Biol. 2006; 16(21):2135–2142. [PubMed: 17084698]

Mishima Y, Tomari Y. Codon Usage and 3′ UTR Length Determine Maternal mRNA Stability in Zebrafish. Mol Cell. 2016; 61(6):874–885. [PubMed: 26990990]

Morris DR, Geballe AP. Upstream open reading frames as regulators of mRNA translation. Mol Cell Biol. 2000; 20:8635–8642. [PubMed: 11073965]

Mugridge JS, Ziemniak M, Jemielity J, Gross JD. Structural basis of mRNA-cap recognition by Dcp1-Dcp2. Nat Struct Mol Biol. 2016; 23(11):987–994. [PubMed: 27694842]

Nitanda Y, Matsui T, Matta T, Higami A, Kohno K, Nakahata Y, Bessho Y. 3′-UTR-dependent regulation of mRNA turnover is critical for differential distribution patterns of cyclic gene mRNAs. FEBS J. 2014; 281(1):146–156. [PubMed: 24165510]

Oates AC, Ho RK. *Hairy/E(spl)-related (Her)* genes are central components of the segmentation oscillator and display redundancy with the Delta/Notch signaling pathway in the formation of anterior segmental boundaries in the zebrafish. Dev. 2002; 129(12):2929–2946.

Oates AC, Mueller C, Ho RK. Cooperative function of *deltaC* and *her7* in anterior segment formation. Dev Biol. 2005; 280(1):133–149. [PubMed: 15766754]

Oates AC, Morelli LG, Ares S. Patterning embryos with oscillations: structure, function and dynamics of the vertebrate segmentation clock. Dev. 2012; 139:625–639.

Palmeirim I, Henrique D, Ish-Horowicz D, Pourquié O. Avian hairy gene expression identifies a molecular clock linked to vertebrate segmentation and somitogenesis. Cell. 1997; 91(5):639–648. [PubMed: 9393857]

Park E, Maquat LE. Staufen-mediated mRNA decay. Wiley Interdiscip Rev RNA. 2013; 4(4):423–435. [PubMed: 23681777]

Peccarelli M, Kebaara BW. Regulation of natural mRNAs by the nonsense-mediated mRNA decay pathway. Eukaryot Cell. 2014; 13(9):1126–1135. [PubMed: 25038084]

Popp MW, Maquat LE. Organizing principles of mammalian nonsense-mediated mRNA decay. Annu Rev Genet. 2013; 47:139–165. [PubMed: 24274751]

Postlethwait JH, Johnson SL, Midson CN, Talbot WS, Gates M, Ballinger EW, Africa D, Andrews R, Carl T, Eisen JS, et al. A genetic linkage map for the zebrafish. Science. 1994; 264(5159):699–703. [PubMed: 8171321]

Pourquié O. Vertebrate segmentation: from cyclic gene networks to scoliosis. Cell. 2011; 145:650–663. [PubMed: 21620133]

Purvis JE, Lahav G. Encoding and decoding cellular information through signaling dynamics. Cell. 2013; 152(5):945–956. [PubMed: 23452846]

Riley MF, Bochter MS, Wahi K, Nuovo GJ, Cole SE. *mir-125a-5p*-mediated regulation of *Lfng* is essential for the avian segmentation clock. Dev Cell. 2013; 24:554–561. [PubMed: 23484856]

Riven I, Kalmanzon E, Segev L, Reuveny E. Conformational rearrangements associated with the gating of the G protein-coupled potassium channel revealed by FRET microscopy. Neuron. 2003; 38(2):225–235. [PubMed: 12718857]

Rupp RA, Snider L, Weintraub H. *Xenopus* embryos regulate the nuclear localization of XMyoD. Genes Dev. 1994; 8:1311–1323. [PubMed: 7926732]

Sachs MS, Geballe AP. Downstream control of upstream open reading frames. Genes Dev. 2006; 20(8):915–21. [PubMed: 16618802]

Sander JD, Maeder ML, Reyon D, Voytas DF, Joung JK, Dobbs D. ZiFiT (Zinc Finger Targeter): an updated zinc finger engineering tool. Nucleic Acids Res. 2010; 1(38, Suppl):W462–468.

Sander JD, Zaback P, Joung JK, Voytas DF, Dobbs D. Zinc Finger Targeter (ZiFiT): An Engineered Zinc Finger/Target Site Design Tool. Nucleic Acids Res. 2007; 35:W599–W605. [PubMed: 17526515]

Schoenberg DR, Maquat LE. Regulation of cytoplasmic mRNA decay. Nat Rev Genet. 2012; 13(4): 246–259. [PubMed: 22392217]

Schwendinger-Schreck J, Kang Y, Holley SA. Modeling the zebrafish segmentation clock's gene regulatory network constrained by expression data suggests evolutionary transitions between oscillating and nonoscillating transcription. Genet. 2014; 197(2):725–738.

Shih NP, François P, Delaune EA, Amacher SL. Dynamics of the slowing segmentation clock reveal alternating two-segment periodicity. Dev. 2015; 142(10):1785–1793.

Somers J, Pöyry T, Willis AE. A perspective on mammalian upstream open reading frame function. Int J Biochem Cell Biol. 2013; 45(8):1690–1700. [PubMed: 23624144]

Sonnen KF, Aulehla A. Dynamic signal encoding–from cells to organisms. Semin Cell Dev Biol. 2014; 34:91–98. [PubMed: 25008461]

Soza-Ried C, Öztürk E, Ish-Horowicz D, Lewis J. Pulses of Notch activation synchronise oscillating somite cells and entrain the zebrafish segmentation clock. Dev. 2014; 141(8):1780–1788.

Subtelny AO, Eichhorn SW, Chen GR, Sive H, Bartel DP. Poly(A)-tail profiling reveals an embryonic switch in translational control. Nature. 2014; 508(7494):66–71. [PubMed: 24476825]

Takahashi K, Kotani T, Katsu Y, Yamashita M. Possible involvement of insulin-like growth factor 2 mRNA-binding protein 3 in zebrafish oocyte maturation as a novel cyclin B1 mRNA-binding protein that represses the translation in immature oocytes. Biochem Biophys Res Commun. 2014; 448(1):22–27. [PubMed: 24735541]

Takashima Y, Ohtsuka T, González A, Miyachi H, Kageyama R. Intronic delay is essential for oscillatory expression in the segmentation clock. Proc Natl Acad Sci USA. 2011; 108:3300–3305. [PubMed: 21300886]

Takeda Y, Mishima Y, Fujiwara T, Sakamoto H, Inoue K. DAZL relieves miRNA-mediated repression of germline mRNAs by controlling poly(A) tail length in zebrafish. PLoS One. 2009; 4(10):e7513. [PubMed: 19838299]

Takke C, Campos-Ortega JA. *her1*, a zebrafish pair-rule like gene, acts downstream of Notch signalling to control somite development. Dev. 1999; 126(13):3005–3014.

Talbot JC, Amacher SL. A streamlined CRISPR pipeline to reliably generate zebrafish frameshifting alleles. Zebrafish. 2014; 11:583–585. [PubMed: 25470533]

Tan SL, Ohtsuka T, González A, Kageyama R. *MicroRNA9* regulates neural stem cell differentiation by controlling *Hes1* expression dynamics in the developing brain. Genes Cells. 2012; 17:952–961. [PubMed: 23134481]

Thermes V, Grabher C, Ristoratore F, Bourrat F, Choulika A, Wittbrodt J, Joly JS. I-SceI meganuclease mediates highly efficient transgenesis in fish. Mech Dev. 2002; 118:91–98. [PubMed: 12351173]

Turner DL, Weintraub H. Expression of *achaete-scute homolog 3* in *Xenopus* embryos converts ectodermal cells to a neural fate. Genes Dev. 1994; 8:1434–1447. [PubMed: 7926743]

Ulitsky I, Shkumatava A, Jan CH, Subtelny AO, Koppstein D, Bell GW, Sive H, Bartel DP. Extensive alternative polyadenylation during zebrafish development. Genome Res. 2012; 22(10):2054–2066. [PubMed: 22722342]

Valkov E, Muthukumar S, Chang CT, Jonas S, Weichenrieder O, Izaurralde E. Structure of the Dcp2-Dcp1 mRNA-decapping complex in the activated conformation. Nat Struct Mol Biol. 2016; 23(6):574–579. [PubMed: 27183195]

von Roretz C, Gallouzi IE. Decoding ARE-mediated decay: is microRNA part of the equation? J Cell Biol. 2008; 181(2):189–194. [PubMed: 18411313]

Wethmar K. The regulatory potential of upstream open reading frames in eukaryotic gene expression. Wiley Interdiscip Rev RNA. 2014; 5(6):765–778. [PubMed: 24995549]

Williams DR, Shifley ET, Braunreiter KM, Cole SE. Disruption of somitogenesis by a novel dominant allele of *Lfng* suggests important roles for protein processing and secretion. Dev. 2016; 143(5): 822–830.

Wittkopp N, Huntzinger E, Weiler C, Saulière J, Schmidt S, Sonawane M, Izaurralde E. Nonsense-mediated mRNA decay effectors are essential for zebrafish embryonic development and survival. Mol Cell Biol. 2009; 29(13):3517–3528. [PubMed: 19414594]

Wright GJ, Giudicelli F, Soza-Ried C, Hanisch A, Ariza-McNaughton L, Lewis J. DeltaC and DeltaD interact as Notch ligands in the zebrafish segmentation clock. Dev. 2011; 138(14):2947–2956.

Wong SF, Agarwal V, Mansfield JH, Denans N, Schwartz MG, Prosser HM, Pourquié O, Bartel DP, Tabin CJ, McGlinn E. Independent regulation of vertebral number and vertebral identity by *microRNA-196* paralogs. Proc Natl Acad Sci USA. 2015; 112(35):E4884–4893. [PubMed: 26283362]

Yasuda K, Kotani T, Ota R, Yamashita M. Transgenic zebrafish reveals novel mechanisms of translational control of cyclin B1 mRNA in oocytes. Dev Biol. 2010; 348(1):76–86. [PubMed: 20883683]

Zhou D, Chen S. PNRC2 is a 16 kDa coactivator that interacts with nuclear receptors through an SH3-binding motif. Nucleic Acids Res. 2001; 29(19):3939–3948. [PubMed: 11574675]

Zhou D, Shen R, Ye JJ, Li Y, Tsark W, Isbell D, Tso P, Chen S. Nuclear receptor coactivator PNRC2 regulates energy expenditure and adiposity. J Biol Chem. 2008; 283(1):541–553. [PubMed: 17971453]

Zhou D, Ye JJ, Li Y, Lui K, Chen S. The molecular basis of the interaction between the proline-rich SH3-binding motif of PNRC and estrogen receptor alpha. Nucleic Acids Res. 2006; 34(20): 5974–5986. [PubMed: 17068076]

Zuker M. Mfold web server for nucleic acid folding and hybridization prediction. Nucleic Acids Res. 2003; 31(13):3406–3415. 2003. [PubMed: 12824337]

Summary statement

Pnrc2 regulates 3′UTR-mediated decay of segmentation clock transcripts during vertebrate segmentation. Pnrc2 loss results in accumulation of cyclic transcripts, but not cyclic proteins.

Author Manuscript
Author Manuscript
Author Manuscript

Highlights

- *pnrc2* promotes decay of cyclic transcripts during segmentation.
- A cyclic 3′UTR confers Pnrc2-dependent instability to a heterologous transcript.
- Cyclic mRNA decay is Dicer-independent.
- Cyclic mRNA decay likely employs a Pnrc2-Upf1-containing mRNA decay complex.
- Cyclic mRNA accumulates in *pnrc2* mutants, but cyclic protein is expressed normally.

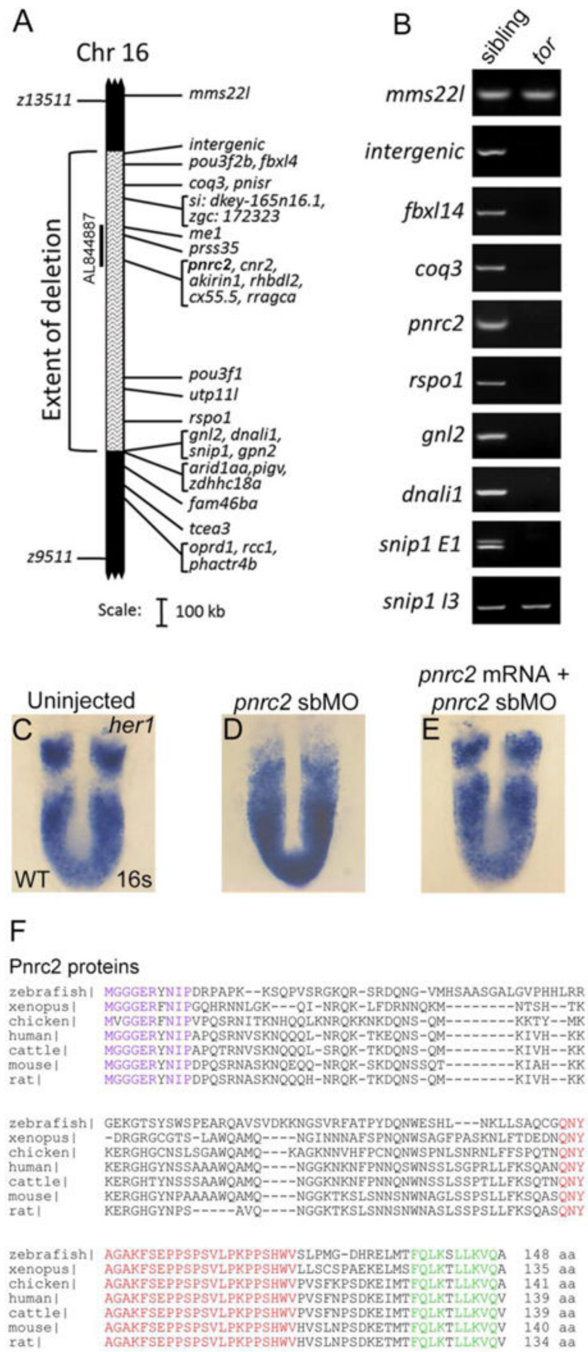

Figure 1. The tortuga^{b644} allele is a 1.46 Mb deficiency that includes the pnrc2 gene

Haploid-based mapping revealed that the *tortuga* lesion lies 0.30 cM to the left (4/1434 recombinants) and 0.37 cM to the right (4/1083 recombinants) of the SSLP markers z13511 and z9511, respectively (A). The extent of the deletion was refined by PCR-based screening of regions within and around the deletion interval from pooled genomic DNA samples of 10 wild-type (WT) and 10 *tortuga* mutant embryos (B); regions that fail to amplify in mutants are deleted in the *tor^{b644}* allele (A, B). Among BACs spanning the deletion interval, only BAC AL844887 restores *her1* expression when injected into *tor* mutants (A; Fig S1A–D). In wild-type embryos, *her1* is expressed in a striped pattern (n=54/54) (C). In contrast, embryos injected with 6 ng of *pnrc2* splice-blocking morpholino (sbMO) have a *tortuga*-like *her1* expression defect (n=37/39) (D). When *pnrc2* mRNA is co-injected with 4 ng *pnrc2* sbMO, *her1* expression is partially restored in a dose-dependent manner (n=3/19 WT *her1* expression, 150 pg *pnrc2* mRNA; n=7/17 WT *her1* expression, 600 pg *pnrc2* mRNA) (E; Table 1). Alignment of vertebrate Pnrc2 amino acid sequences reveals a conserved 10 amino acid N-terminus (purple) and conserved C-terminal SRC-Homology 3 (SH3) (red) and Nuclear Receptor (NR box) domains (green) (F). Clustal alignments were performed in consultation with published alignments for vertebrate Pnrc2 (Valkov et al, 2016).

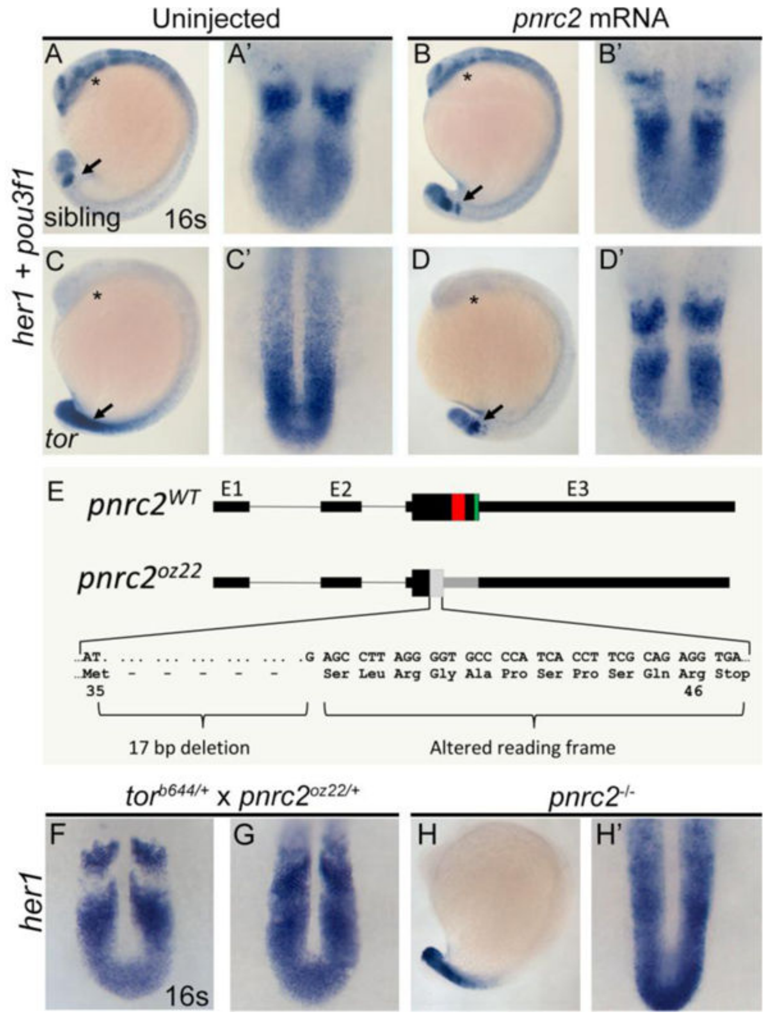

Figure 2. tor mutant embryos are rescued by injection of pnrc2 mRNA and phenocopied by frame-shifting mutation of the pnrc2 locus

Injection of 100 pg *pnrc2* mRNA has no effect in wild-type sibling embryos (n=15/15 non-mutant siblings) (A, A′ vs B, B′) but restores striped *her1* expression in *tor* mutant embryos (n=10/10 mutants) (C, C′ vs D, D′; Table 2). In these experiments, rescued *tor*^{b644} mutant embryos were distinguished from wild-type siblings by lack of expression of *pou3f1*, a gene located in the *tor*^{b644} deficiency interval. Asterisks (*) mark the neural *pou3f1* expression domain. Arrows mark the *her1* expression domain (A–D), magnified in dorsal view to the right of each embryo (A′–D′). Using CRISPR-based mutagenesis, we induced a 17 bp deletion within the *pnrc2* coding sequence, creating an early frameshift allele, designated *pnrc2*^{oz22} (E). Predicted mutant protein sequence is based on sequenced genomic DNA (E). The *pnrc2*^{oz22} allele fails to complement the *her1* accumulation phenotype of the *tor*^{b644} deletion allele (n=4/15 embryos from a heterozygote intercross with *tor*-like *her1* accumulation) (F, G). Similar to *tor*^{b644} mutants, *pnrc2*^{oz22} mutant embryos lack a striped *her1* expression pattern (H, ′H).

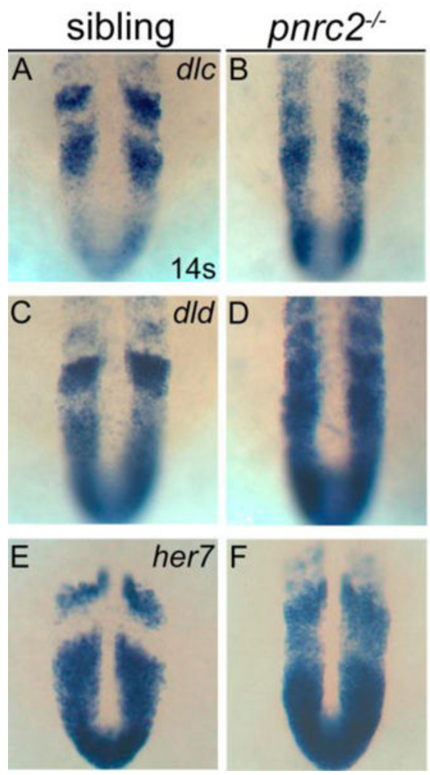

Figure 3. Segmentation clock transcripts accumulate in pnrc2 mutant embryos

Like *her1*, other segmentation clock genes, *dlc* (A, B), *dld* (C,D), and *her7* (E, F), are misexpressed in *pnrc2* mutant embryos, with expression detected throughout the presomitic mesoderm (PSM) in the expected one-quarter of embryos in a $pnrc2^{oz22}$ intercross, n=8/25 (X^2=0.65, p=0.4), 6/25 (X^2=0.013, p=0.9), and 8/25 (X^2=0.65, p=0.4), respectively (A–F).

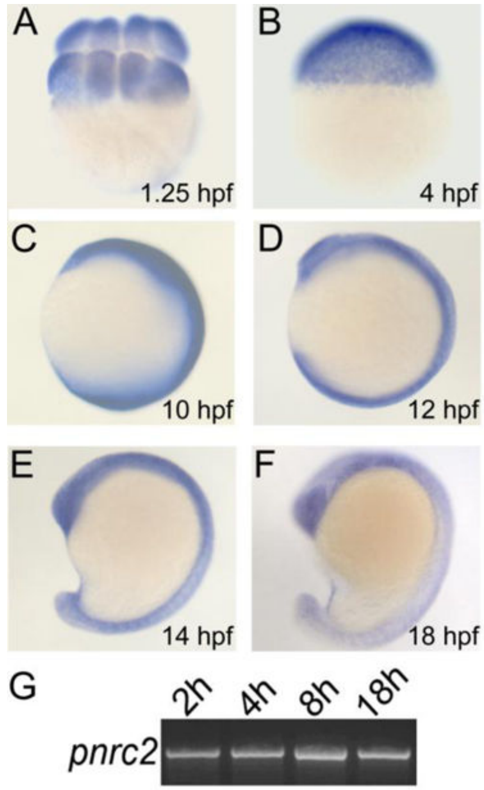

Figure 4. pnrc2 is broadly expressed during segmentation stages

pnrc2 transcripts are detected during early embryonic stages and throughout segmentation stages by in situ hybridization (n>15 per time point) (A–F). As expected, there is no detectable staining with a *pnrc2* sense probe (n=15/15) (data not shown). RT-PCR expression analysis for *pnrc2* at 2 hours post fertilization (2h) through mid-segmentation (18h) is consistent with in situ detection of *pnrc2* transcript (see Methods and Results) (G).

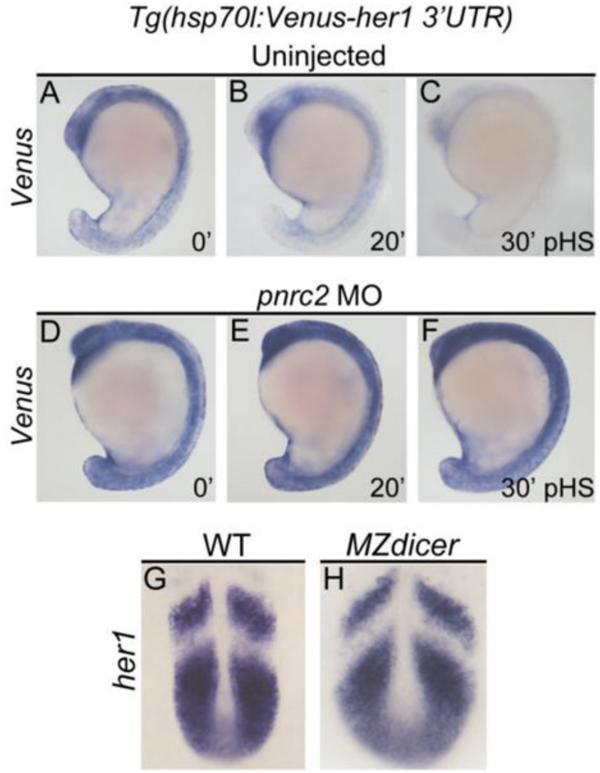

Figure 5. Pnrc2-mediated decay functions via 3′UTR recognition and does not require Dicer-dependent miRNAs

Stably transgenic embryos carrying the *hsp70l:Venus her1* 3′UTR reporter were injected at the 1-cell stage with *pnrc2* sbMO or reserved as uninjected controls. Embryos were then raised to mid-segmentation stage, heat-shocked for 15 minutes, then collected at the indicated minutes post-heat-shock (pHS) and processed by *Venus* in situ hybridization (n=65, 6 ng *pnrc2* sbMO; n=55, uninjected controls) (A–F). *Venus* transcripts are not detected in the absence of heat-shock (n=10) (not shown). To determine whether Dicer-generated miRNAs contribute to *her1* mRNA decay, *MZdicer* mutants (n=11) and wild-type controls (n=10) were raised to mid-segmentation stages (16–18 hpf) and processed by *her1* in situ hybridization (G, H). At this timepoint, *MZdicer* mutants are developmentally delayed relative to wild-type controls (Giraldez et al, 2005), and thus have a different overall shape.

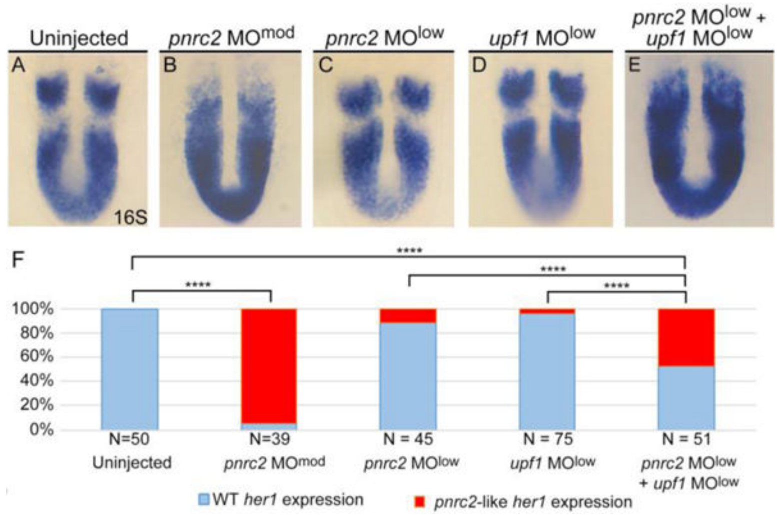

Figure 6. pnrc2 and the nonsense-mediated decay effector Upf1 promote decay of cyclic mRNA

Injection of low dose *pnrc2* sbMO (2 ng) has little to no effect on *her1* expression (A, C), contrasting with the expected *her1* misexpression observed after injection of moderate dose *pnrc2* sbMO (6 ng) (B). Low dose injection of *upf1* sbMO (0.25 ng) also has little effect on *her1* expression (D), but when combined with a low dose of *pnrc2* sbMO (2 ng), *her1* misexpression is observed in about 50% of injected embryos (E). The proportion affected in each condition is plotted on a bar graph that indicates significant differences between single morphants, double morphants, and controls (F). sbMO = splice-blocking MO; **** = p<0.0001.

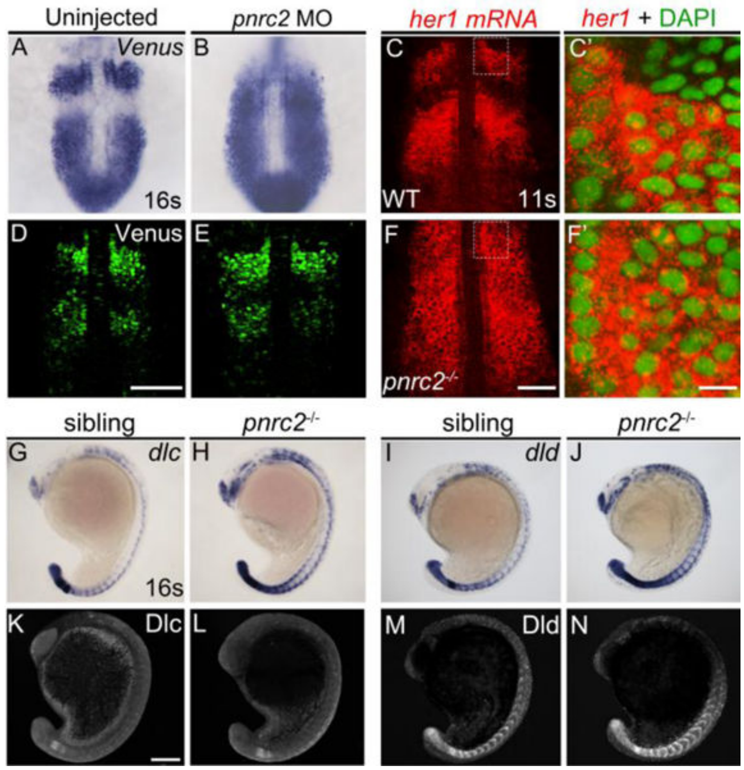

Figure 7. Both reporter and endogenous cyclic transcripts accumulate in Pnrc2-depleted embryos, but protein expression appears normal

Embryos carrying the *her1:her1-Venus*^{bk15} transgenic clock reporter were injected with *pnrc2* splice-blocking morpholino (sbMO) and processed to detect *Venus* transcripts (A, B) and Venus protein (D, E) at mid-segmentation stages. Representative embryos are shown in A (n=21/21); B (n=18/18), D (n=32/32), and E (n=29/29). Venus immunofluorescence panels (D, E) are at slightly higher magnification than *Venus* in situ panels (A, B). Detection of *her1* mRNA by in situ hybridization chain reaction (HCR-ISH) (C, F) is consistent with chromogenic NBT/BCIP-based in situ detection of endogenous *her1* transcript in wild-type and *pnrc2* mutant embryos (Fig 2F, H′), with substantial cytoplasmic localization revealed by DAPI counter staining in 500X magnified view (C′, F). Because relative intensity of *her1* HCR-ISH in *pnrc2* mutants to wild-type embryos is high, levels have been reduced in *pnrc2* mutant panels (F–F; see Fig S6A‴, B‴). Misexpression of *dlc* and *dld* mRNA is detected throughout the presomitic mesoderm (PSM), formed somites and neurons in the expected one-quarter of embryos in a *pnrc2*^{oz22} intercross, n=5/28 (X^2=0.76, p=0.4) and n=7/40 (X^2=1.2, p=0.3), respectively (G–J). In contrast, Dlc and Dld protein expression is indistinguishable among siblings of the same *pnrc2*^{oz22} heterozygote intercross (K–N). Dlc and Dld immunolabeled embryos were genotyped prior to imaging and a subset of wild-type and mutant siblings were imaged by confocal microscopy with representative embryos shown (K–N). Total genotyped individuals per representative panel: n=5 (K), n=6 (L), n=12 (M), n=4 (N). Scale bars = 50 um (D, F), 50 nm (F′), 100 um (K).

Table 1

Injection of pnrc2 mRNA partially restores normal her1 expression in pnrc2 morphants

Condition	*her1* expression[a]		
	Normal	**Partial *tor*-like**	***tor*-like**
Uninjected WT	54/54 (100%)	0/54 (0%)	0/54 (0%)
4 ng *pnrc2* sbMO	2/39 (5%)	28/39 (72%)	9/39 (23%)
4ng *pnrc2* sbMO + 150 pg *pnrc2* mRNA[b]	3/19 (16%)	12/19 (63%)	4/19 (21%)
4 ng *pnrc2* sbMO + 600 pg *pnrc2* mRNA[b]	7/17 (42%)	9/17 (53%)	1/17 (6%)

[a]Wild-type embryos were injected at the 1-cell stage with 4 ng *pnrc2* sbMO with and without increasing doses of MO-resistant *pnrc2* mRNA, raised to 16–18 hpf, and processed by *her1* in situ hybridization. Normal, *her1* is expressed in visible stripes separated by regions of low expression; Partial *tor*-like, *her1* stripes are distinguishable, but there is substantial *her1* detected between stripes; *tor*-like, *her1* expression is strong throughout the PSM with no obvious peaks or troughs.

[b]Chi-square analysis indicates a significant difference in *her1* expression between *pnrc2* morphants with and without co-injection of *pnrc2* mRNA. Co-injection of 150 pg and 600 pg of *pnrc2* mRNA significantly restores *her1* expression in morphants ($p<2.1 \times 10^{-3}$ and $p<8.8 \times 10^{-8}$, respectively).

Table 2

Injection of pnrc2 mRNA restores normal her1 expression in tor^{b644} mutants

mRNA dose (pg)	Live Embryonic Phenotype		WT *her1* ISH/ WT genotype[b]	WT *her1* ISH/ *tor* genotype[b]	*tor her1* ISH/ *tor* genotype[b]
	WT[a]	Neural degen[a]			
0	103	31	103/103	0/31	31/31
75	64	20	64/64	19/20[c]	1/20[d]
100	15	10	15/15	10/10[c]	0/10[d]

[a]At the 16–18 somite stage, *pnrc2* mRNA-injected embryos from a *tor*^{b644} heterozygote intercross were scored for neural degeneration, a non-somitic phenotype observed in *tor* mutants.

[b]After sorting by live phenotype, injected embryos were processed by *her1* in situ hybridization to assess phenotypic rescue and with *pou3f1* to identify individuals homozygous for the *tor* deletion. Representative embryos are shown in Fig 2.

[c]Both 75 and 100 pg doses correlate with restoration of normal *her1* expression. At the 100 pg dose, all *tor* mutants have a normal *her1* expression pattern.

[d]Chi-square analysis indicates a significant difference in *her1* expression among *pnrc2* mRNA-injected *tor* mutants compared to uninjected homozygous siblings ($p<4.7 \times 10^{-7}$ and $p<3.9 \times 10^{-3}$, for 75 pg and 100 pg doses, respectively).

Table 3

Pnrc2 is required for the transcript destabilizing effect of the her1 3′UTR

***hsp70l:Venus-her1* 3′UTR Condition**[a]	**pHS recovery time**[b]	**Expression Level**[c]			**Number of embryos**	**Mean Expression**
		3	**2**	**1**		
Uninjected	0	20	0	4	24	2.7[d]
6 ng *pnrc2* MO	0	27	0	0	27	3.0[d]
Uninjected	20	0	0	6	6	1.0[d]
6 ng *pnrc2* MO	20	11	0	0	11	3.0[d]
Uninjected	30	0	8	17	25	1.3[d]
6 ng *pnrc2* MO	30	27	0	0	27	3.0[d]

[a]A stably transgenic male carrying a *hsp70l:Venus-her1* 3′UTR reporter was crossed to a wild-type female; half of the progeny were injected with *pnrc2* sbMO and the other half used as uninjected sibling controls.

[b]At 14–16 hpf, embryos were heat-shocked at 37°C for 15 minutes, followed by fixation at indicated post-heat shock (pHS) recovery times.

[c]Fixed embryos were processed and scored as described in Table 1. Embryos completely lacking *Venus* expression were not included because we could not discriminate the expected 50% of embryos that did not inherit the transgene from transgenic embryos lacking detectable *Venus* expression.

[d]Average expression levels reveal that *pnrc2* MO-injection into transgenic embryos dramatically stabilizes *Venus* transcript levels post heat-shock across the recovery time course of 30 minutes when compared to uninjected controls.

Table 4

pnrc2 mutants segment normally

	Genotype		
Feature	**Wild type**	***pnrc2***$^{+/-}$	***pnrc2***$^{-/-}$
Segment number	34.7 ± 0.7 (n = 14)	35.3 ± 0.3 (n = 14)	34.3 ± 0.4 (n = 14)

Sibling embryos from a *pnrc2oz22* heterozygote intercross were raised to 36 hpf and processed by *cb1045 (xirp2a)* in situ hybridization that reliably marks segment boundaries. PCR-based genotyping was performed for individuals after in situ hybridization and segment counts. No significant differences were observed between genotypes. Segment numbers are given as mean ± 95% confidence interval (Student's t test).